RSC Advances

ROYAL SOCIETY OF CHEMISTRY

www.rsc.org/advances

Journal Name ARTICLE

TD-DFT calculations of UV absorption bands and their intensities in the spectra of some tetrahydroquinolines.

María V. Cooke,[a] Ivana Malvacio,[a] Walter J. Peláez, [a,] * Ana J. Pepino,[a] María R. Mazzieri,[b] and Gustavo A. Argüello[a]

[a] INFIQC-Dpto. de Fisicoquímica, Facultad de Ciencias Químicas, UNC, Córdoba, 5000, Argentina.[b] Dpto. de Farmacía, Facultad de Ciencias Químicas, UNC, Córdoba, 5000, Argentina.
E-mail: waldemar31@fcq.unc.edu.ar

Table of contents

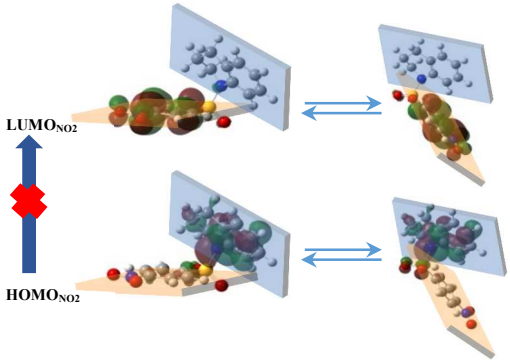

Text of Table of contents

A detailed analysis of the MOs involved in electronic transitions of 1-benzenesulfonyl-1,2,3,4-tetrahydroquinolines are presented for the first time.

Cite this: DOI: 10.1039/x0xx00000x

TD-DFT calculations of UV absorption bands and their intensities in the spectra of some tetrahydroquinolines.

María V. Cooke,[a] Ivana Malvacio,[a] Walter J. Peláez,[a,*] Ana J. Pepino,[a] María R. Mazzieri,[b] and Gustavo A. Argüello[a]

Received 00th January 2012,
Accepted 00th January 2012

DOI: 10.1039/x0xx00000x

www.rsc.org/

A detailed analysis of the MOs involved in electronic transitions in UV spectra as well as a conformational study of 1-benzenesulfonyl-1,2,3,4-tetrahydroquinoline (BSTHQs) derivatives has been carried out using the TD-DFT (B3LYP/6-31+G(d,p)) method. Based on experimental solvent effects and theoretical investigations the long-wavelength bands have been assigned to π → π* transitions caused by HOMO-LUMO intramolecular charge transfer from the tetrahydroquinoline fragment (THQ) to the benzenesulfonyl moiety (BS). Nevertheless, for the NO_2 derivative the HOMO-LUMO transition was found to be forbidden. In this case the long-wavelength band has been associated to an n → π* transition. Good correlation of theoretical and experimental data for the energy transitions and the molar extinction coefficients of the compounds studied has been obtained and are presented for the first time.

Introduction

1,2,3,4-tetrahydroquinoline (THQ, **1**) and Benzenesulfonyl (BS) derivatives are structures with well known biological activities. The THQ moiety is present in compounds with diverse characteristics such as antimalarial[1] and anticancer activity,[2] nonsteroidal glucocorticoid receptor ligands,[3] agonists of β3 adrenergic receptors,[4] and histamine H3 receptor antagonists,[5] among others. On the other hand, the BS group is a substituent frequently present in biologically active molecules,[6-8] where the presence of the BS group leads to analogues with similar or better biological activities than their precursors.[9] In particular, we demonstrated that 1-benzenesulfonyl-1,2,3,4-tetrahydroquinolines (BSTHQs **2-5**, Figure 1) which are a combination of these active moieties, possess interesting properties as antiparasitic activity,[10] while others have shown different behaviors as HIV-transcriptase inhibitors,[11] low potency calcium channel antagonist[12] and gonadotropin releasing hormone antagonist,[13] respectively.

As part of our ongoing project on N-benzenesulfonyl derivatives as bioactive heterocyclic compounds, our research has been focused on exploring the consequences of a BS-N linkage on the stereoelectronic properties of some 1-benzenesulfonyl-1,2,3,4-tetrahydroquinolines (**2-5**, Figure 1). Experimental (UV-Vis) and theoretical calculations TD-DFT(B3LYP/6-31+G(d,p)[14,15] and CAM-B3LYP/6-31+G(d,p)[16,17]) have been carried out aiming to determine the nature of electronic transitions and their dependences. The selection of the species under study was mainly guided by electronic considerations going from electron-donating, such as $-NH_2$, to electron-withdrawing, such as $-NO_2$ (as defined by the Hammet constant, σ[18]).

Studying the electronic structure by UV spectral and quantum chemical methods is important, not only for interpretation of the spectra, but also to estimate the direction of the electronic density redistribution of the compounds, which is a determining factor of their reactivity and biological activity.

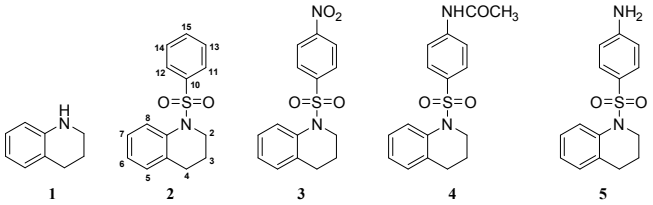

Figure 1. 1,2,3,4-tetrahydroquinoline (THQ, **1**) and 1-benzenesulfonyl-1,2,3,4-tetrahydroquinolines derivatives (BSTHQs **2-5**) studied in the present work.

Results and discussion

Conformational analysis

In a previous work,[10] we performed some conformational analysis on THQ **1** and BSTHQs **2-5** with the semiempirical (AM1) and DFT (B3LYP/6-31G(d)) methods, as implemented in Gaussian 03. New calculations here confirm the proposed conformational structures established by Charifson *et al.*[8] where the THQ **1** was found to present two equivalent half-chair conformations, while the half-boat conformations were not stable (Figure 2).

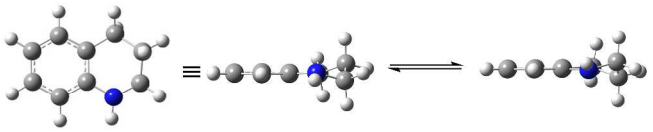

1

Figure 2. Structure of 1,2,3,4-tetrahydroquinoline (THQ, **1**) at DFT(B3LYP/6-31G+(d,p)).

The new calculations presented here (BSTHQs at DFT-B3LYP/6-31+G(d,p) method) deal particularly with the contribution of each conformer to the total UV spectrum in the different solvents. New careful geometry optimizations were performed to establish the position of the BS group and the relative populations of the different conformers in solution (acetonitrile ACN, ethanol EtOH and dichloromethane DCM) to determine which one contributes more to the electronic spectrum.

For BSTHQs, scans of the two relevant dihedral angles were used to inspect the positioning of sulfonyl (α dihedral) and phenyl (β dihedral) substituents. Two minimum-energy conformations for each BSTHQ derivative were found and characterized as stationary points by vibrational frequency calculations. For all BSTHQ **2-5**, the BS group was shown to be in pseudo-axial position, while the phenyl substituent adopts two different (*-in* and *-out*) configurations (Scheme 1) with relative populations given by the Boltzmann distribution which are presented in Table S1(Supp. Inf).

The scheme also shows both the HOMO and the LUMO orbitals in an attempt to rationalize (as it will be discussed later), from a geometrical point of view, the lowest allowed transition in the UV spectrum.

For BSTHQ **2**, the *-in* configuration amounted to 68.6%, while for the others (**3-5**) were higher than 85% (91.3, 90.9 and 88.2% respectively). Calculations of specific NBO (Natural Bond Order) donor-acceptor interactions were performed in order to explain these differences. The explanation lies mainly on the effective energy interaction between the $\pi^*_{C10\text{-}C12}$ antibonding orbital of the phenyl ring and the two π^* orbitals that involve C_{11}-C_{13} and C_{14}-C_{15}, which are present only in the conformers with *-in* conformation of compounds **3-5**.

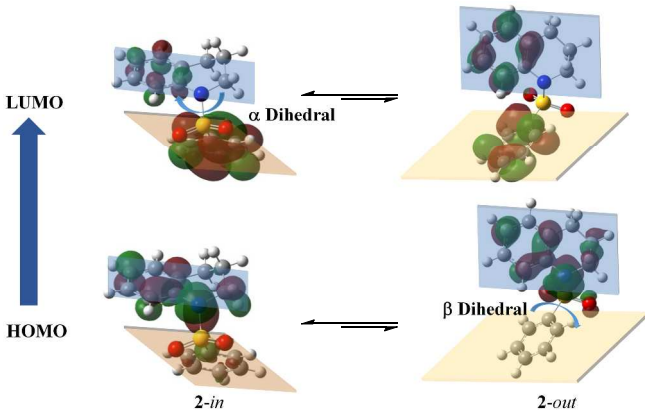

Scheme 1. Two minimum-energy conformations of BSTHQ **2** at DFT (B3LYP/6-31G+(d,p)) method in ACN.

Analysis of MO formation

In Figures 3-4 the type, energy and shapes of MOs of THQ **1** and BSTHQ **2-5** in ACN solvent are presented. The MOs compositions were calculated using the GaussSum software[19].

In compounds **2-5**, the occupied orbitals are mainly localized on the tetrahydroquinoline fragment while the unoccupied orbitals have their major contribution from the phenyl ring. These results suggest that all the transitions involve charge transfer from the thetrahydroquinoline to the phenyl moiety.

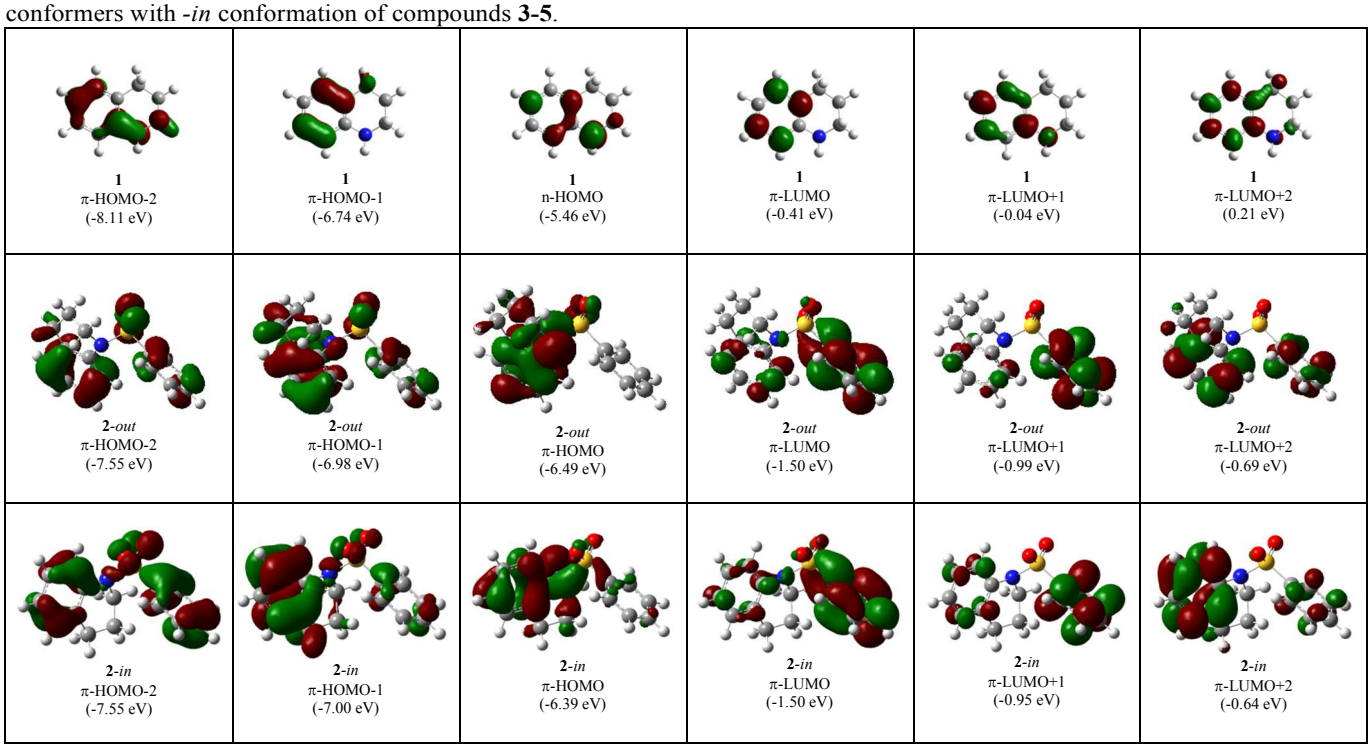

Figure 3. The type, energy (in parenthesis) and shapes of MOs of THQ **1** BSTHQ **2** in ACN solvent by DFT(B3LYP/6-31G+(d,p)) method.

The highest occupied MO (HOMO) of THQ nucleus **1** has mainly *n*-symmetry and is localized on the nitrogen atom (61%). The other orbitals shown (HOMO-2, HOMO-1, LUMO, LUMO+1 and LUMO+2) have π-symmetry localized on the benzene ring (>60%) and the nitrogen atom (~30%), Figure 3.

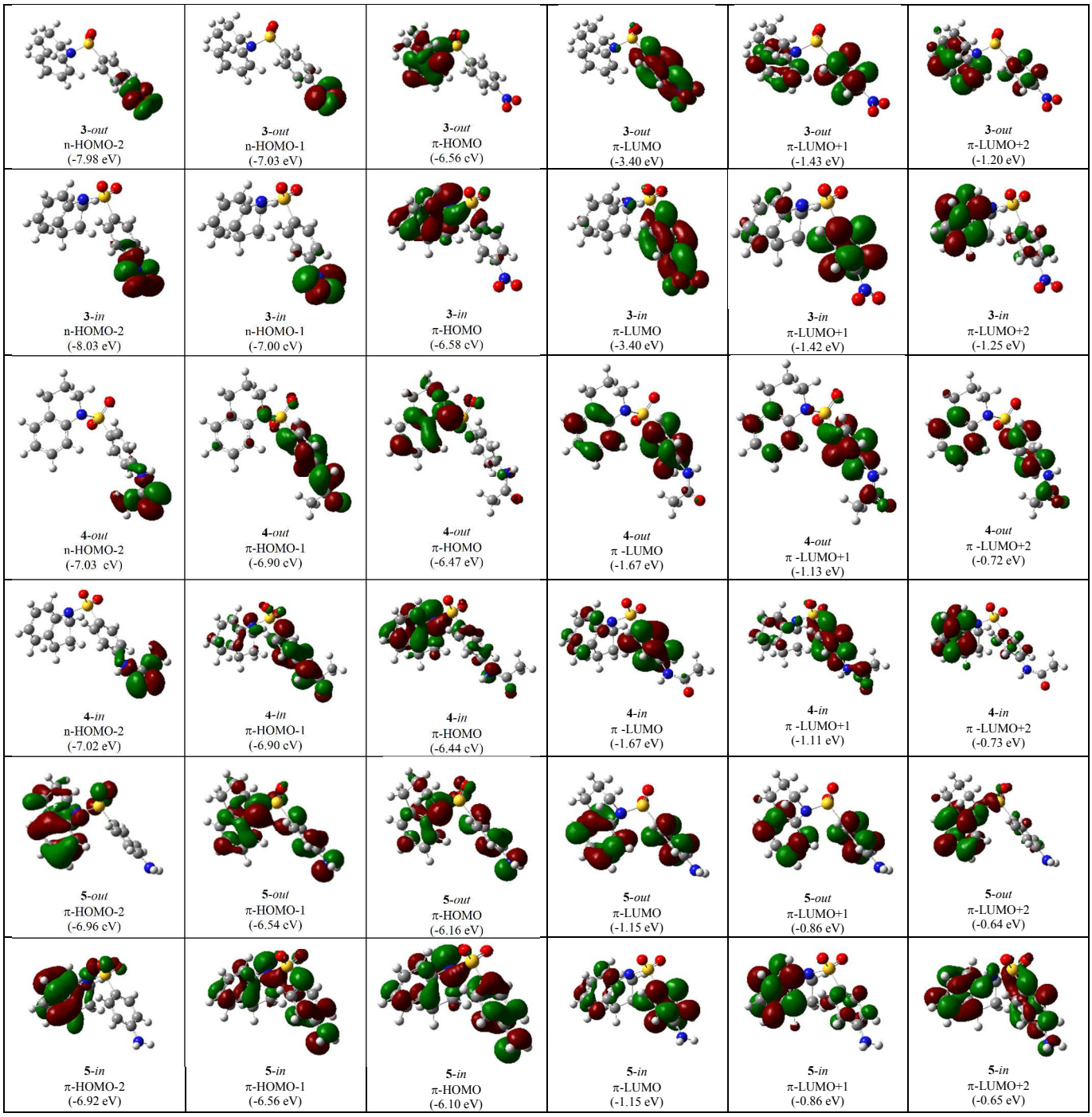

Figure 4. The type, energy (in parenthesis) and shapes of MOs of BSTHQ **3-5** in ACN solvent by DFT(B3LYP/6-31G+(d,p)) method.

For compounds **2-5**, the HOMO has π-symmetry with the main contribution from the tetrahydroquinoline fragment and some from the phenyl ring (**2**: 93/7%, **3**: 93/6%, **4**: 59/23% and **5**: 88/3% Figures 3 and 4). The second-highest occupied MO (HOMO-1) is also π-symmetry in all cases except for compound **3** in which it has n-symmetry localized on the substituent -NO_2 of BS moiety (>60%). Nevertheless, the symmetry of HOMO-2 MOs for all BSTHQ

depend strongly on the substituent in the BS moiety. In the cases where the substituent possess more than one heteroatom with free electron pairs, the MOs have an n-type symmetry localized on the heteroatoms, particularly on the oxygen (**3**: -NO_2 fragment, 60%; **4**: -NH-$COCH_3$, 75%). Meanwhile, for BSTHQ **2** and **5**, the symmetry of the HOMO-2 MOs is π-type and have a significant contribution from the quinoline fragment (97%).

On the other hand, the lowest unoccupied MO (LUMO), LUMO+1 and LUMO+2 have π-symmetry for all BSTHQ (Figure 3-4). LUMO and LUMO+1 are mostly localized on the BS group with the exception of compound **5** in the *-in* conformation where LUMO+1 is localized on the tetrahydroquinoline moiety. LUMO+2 MOs are also localized on the tetrahydroquinoline moiety, with exception of conformers **4**-*out* and **5**-*in* where these are localized ~50 percent on each fragment.

UV measurements

The UV spectra were recorded in ACN, EtOH and DCM in order to obtain information about the nature of the transitions involved in the main bands, Figure 5.

As it can be seen all compounds present three distinctive absorption regions that will be roughly named short (190-220 nm), medium (220-280 nm) and long (280-360 nm) wavelength regions.

In the short wavelength region, all compounds present the most intense band. At longer wavelengths, the THQ nucleus (**1**) manifests two broad bands in the medium and long regions. The N-substitution by the BS group yields compound **2**, which has a less structured spectrum with two weak broad bands in the medium region between 220-250 nm and 260-280 nm. Compound **3** presents a spectrum similar to **2**, while **4** and **5** exhibit an intense band with its maximum at ~270 nm.

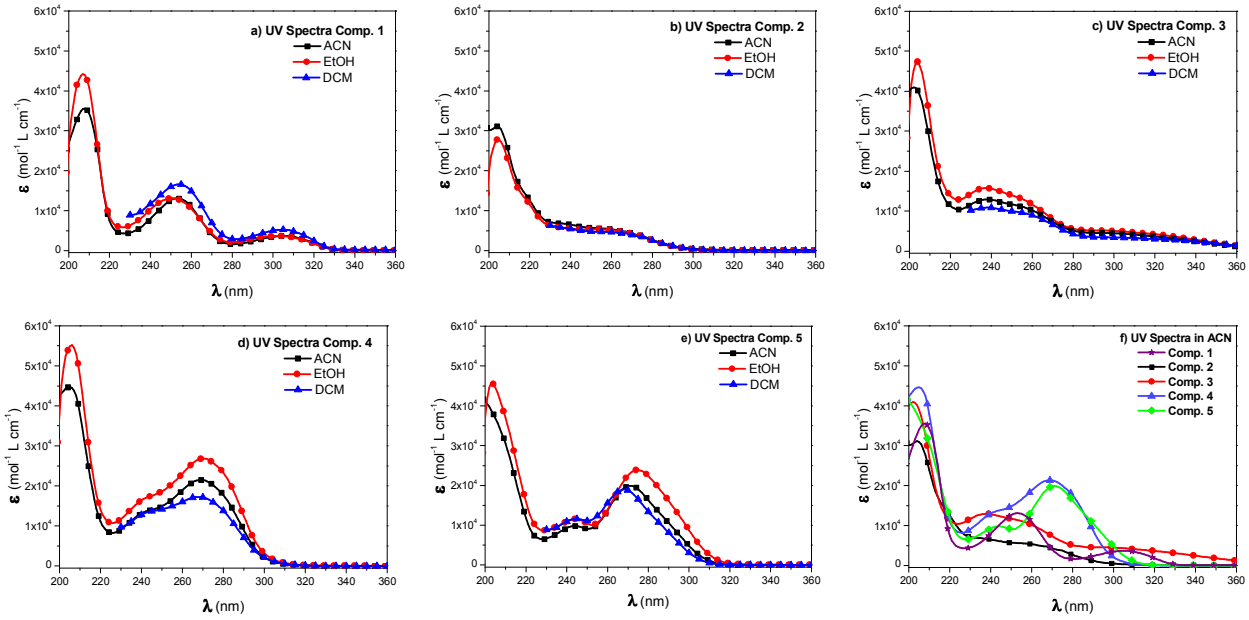

Figure 5. a-e) UV spectra of compounds **1-5** in EtOH, ACN and DCM. f) UV spectra of compounds **1-5** in ACN.

The λ max at ~270 nm of compounds **4** and **5** moves to longer wavelenghts (bathochromic shift) in solvents of increasing polarity which suggests that it could be associated to a π → π* transition, Table 1. Otherwise, the corresponding band in compound **3** (~293 nm) shows the opposite behavior which could be associated to a n → π* transition. Table 1 lists experimental λ_{max} (nm) and ε (M^{-1} cm^{-1}), where the blue arrows show the shifting in wavelengths while the red ones mark the changes in intensity with the change in polarity of the solvent.

In addition, no clear solvent effects were observed for the other absorption maxima of **1** and **2**, which would suggest that these are not pure transitions, but combinations.

Table 1. λ_{max} (nm) and ε (M^{-1} cm^{-1}) of compounds **1-5** in different solvents.

Compound	Media	Wavelength (nm) / ε (M-1 cm-1)		
1	DCM	305 / 6300	254 / 19200	-
	ACN	305 / 3650	253 / 12840	208 / 34100
	EtOH	302 / 3510	250 / 12500	207 / 40000
2	DCM	258 / 5300	-	-
	ACN	258 / 5790	219 / 14200	204 / 32100
	EtOH	258 / 6550	220 / 12800	204 / 27900
3	DCM	294 / 4580	238 / 11900	-
	ACN	293 / 4650	238 / 13240	202 / 39000
	EtOH	292 / 5060	237 / 17500	204 / 41000
4	DCM	268 / 20200	241 / 15500	-
	ACN	269 / 21780	240 / 13200	205 / 44500
	EtOH	270 / 27200	240 / 16500	206 / 51600
5	DCM	268 / 20400	245 / 12600	-
	ACN	271 / 20600	244 / 10460	199 / 40400
	EtOH	275 / 23100	244 / 11360	204 / 40800

UV calculations

TD-DFT calculations were used to simulate the UV spectra and to determine the MOs involved in each transition. These calculations were performed in ACN, EtOH and DCM with B3LYP and CAM-B3LYP functional methods since it is known that having transitions with charge transfer character, the latter method should perform better

After analyzing the lowest optically active excitation energy for the most abundant conformer of compounds **2-5**, there was not a clear trend in the shifting of the bands with the solvent, as can be seen in Table S3 of the Supp. Inf. The CAM-B3LYP functional method was appropriate to describe the positioning of the absorption bands for compound **3** (providing a wavelenght value closer to the experimental one) though did not show any trend with the change of polarity in the solvent.

Table 2. Experimental (ACN) and theoretical (TD-DFT) characteristics of studied compounds **1-5**.

Entry	Compound (% *in/out*)	Experimental[a]		Calculated (TD DFT)[b]						Transition[c]	Assignament
				in			*out*				
		$\lambda_{max}^{exp}(nm)$	ε_{exp}	$\lambda_{max}^{calc}(nm)$	*f*	ε_{cal}	$\lambda_{max}^{calc}(nm)$	*f*	ε_{cal}		
1	**1** (50/50)	208	34100	200	0.177	11923	200	0.177	11923	H-1→L+2	π→π*
2				204	0.237	16005	204	0.237	16005	H-1→L	π→π*
3				205	0.195	13137	205	0.195	13137	H-1→L+1	π→π*
4		253	12840	247	0.125	8401	247	0.125	8401	H→L+2	n→π*
5		305	3650	287	0.064	4339	287	0.064	4339	H→L	n→π*
6	**2** (54/46)	204	32100	201	0.068	4602	199	0.180	12119	H-2→L+2/ H-2→L+1	π→π*
7				205	0.050	3360	208	0.106	7119	H→L+5/ H-1→L+3	π→π*
8		219	14200	211	0.162	10924	222	0.097	6572	H-1→L+2/ H-2→L	π→π*
9				219	0.076	5115	225	0.107	7240	H-3→L/ H-1→L+1	π→π*
10		237	7190	236	0.046	3070	237	0.036	2463	H-2→L	π→π*
11				238	0.047	3198	241	0.156	10533	H→L+3/H→L+2	π→π*
12		258	5790	245	0.049	3320	257	0.029	1937	H→L+2/H→L+1	π→π*
13		271	4350	292	0.176	11869	288	0.023	1572	H→L	π→π*
14	**3** (91/9)	202	39000	202	0.157	10567	204	0.069	4656	H-2→L+1	n→π*
15				208	0.176	11862	207	0.253	17098	H-1→L+4	n→π*
16				210	0.076	5101	211	0.073	4953	H→L+5	π→π*
17		238	13240	235	0.052	3482	238	0.161	10884	H→L+4	π→π*
18		253	11630	261	0.098	6586	271	0.181	12186	H→L+2/H-1→L+2	π→π*/n→π*
19		257	10910	265	0.126	8482	-	-	-	H→L+2/H-4→L	π→π*/π→π*
20		294	4590								
21		302	4540	297	0.230	15513	300	0.190	12840	H-2→L	n→π*
22		305	4440								
23		310	4300								
24		-	-	454	0.064	4318	459	0.025	1694	H→L	π→π* (optically inactive)
25	**4** (90/10)	205	44500	205	0.277	14952	205	0.146	7897	H-2→L+3	n→π*
26				215	0.111	5970	214	0.152	8210	H-4→L	π→π*
27		240	13200	240	0.085	4594	242	0.115	6202	H→L+2	π→π*
28				256	0.371	20000	257	0.170	9193	H-2→L	n→π*
29				265	0.062	3368	263	0.463	24966	H-1→L	π→π*
30		269	21780	297	0.297	16037	297	0.083	4459	H→L	π→π*
31	**5** (87/13)	199	40400	198	0.131	8859	200	0.121	8164	H-4→L/ H-3→L+1	π→π*
32		205	37400	208	0.213	14365	208	0.099	6694	H-2→L+3	π→π*
33				209	0.109	7355	212	0.211	14217	H→L+6/ H-3→L	π→π*
34		212	27500	214	0.114	7672	213	0.062	4150	H-3→L/ H-2→L+2	π→π*
35		244	10460	245	0.088	5918	232	0.067	4501	H-1→L+1/ H-1→L+2	π→π*
36				247	0.084	5702	259	0.304	20539	H-1→L+1/ H-1→L	π→π*
37		271	20600	283	0.316	21342	278	0.127	8590	H→L	π→π*

[a]Peak maxima were determined using a second derivative based method.
[b]TD-B3LYP 6-31+G(d,p).
[c]H-highest occupied MO (HOMO), L-lowest unoccupied MO (LUMO).

The experimental maxima and calculated UV spectral data of **1-5** in ACN solvent are given in Table 2. The experimental absorption maxima were determined with the aid of the second derivative spectra. From the analysis of the results, we conclude that the bands in the short wavelength region are a combination of different transitions, as it was expected from solvent effects.

On the other hand, the maximum at the longest wavelength region in compounds **4** and **5** corresponds to the HOMO → LUMO transition which has a π → π* nature caused by intramolecular charge transfer from the quinoline to the BS group (entries 30 and 37, Table 2). This is also in agreement with the bathochromic shift observed in polar solvents

The most remarkable result lies on compound **3**. The calculated TD-B3LYP π → π* HOMO → LUMO transition occurs at longer wavelengths (~454 nm) (entry 24, Table 2). The TD-CAM-B3LYP functional method[16,17] gave a more realistic value with the transition appearing at ~297 nm. This π → π* transition does not seem to be in agreement with the results obtained from the solvent effects, where it was said to be a n → π* transition. Comparing the oscillator strengths (*f*) of the HOMO-LUMO transition between **3** (entry 24, Table 2) and **2**, **4** and **5** (-*in* conformation, entries 13, 30 and 37, Table 2), the former is approximately five times smaller. Therefore, the n → π* nature of the long wavelength transition does not arise from the HOMO → LUMO transition but it comes from the HOMO-2 → LUMO excitation (*f* = 0.230, entry 21, Table 2), in agreement with the solvent effects.

Further analysis of the MOs for compounds **3** to **5** have shed some light as to why HOMO → LUMO appears to be optically inactive (*f* = 0.064) for **3**. HOMO of **4** and **5**, allows us to see that there is a contribution to this orbital from the phenyl ring of the BS moiety that is absent for **3** (-*in* conformation, Figure 4). In the same way, for the LUMO there is a contribution from the aromatic ring of the quinoline moiety for compound **4** and **5** that does not occur for the LUMO of **3**. These differences indicate that the intramolecular charge transfer for **4** and **5** is not pure for the HOMO-LUMO transition compared to what happens in **3**. Nevertheless, there is a substantial contribution from the substituent NO_2 (59%) to the LUMO of **3**, while no contribution to the LUMO of **4** and **5** from the corresponding substituent was observed. This is the reason of the underestimation of the energy in this transition, as it is known for TD-B3LYP calculations. In Figure 6, we present the relative energy of MOs highlighting the transitions that contribute to the experimental bands that appear at the long wavelength region of the UV spectra. It is noteworthy that only for **3**, the contribution comes from one transition while for **2**, **4** and **5** there is a general pattern of three transitions very close in energy.

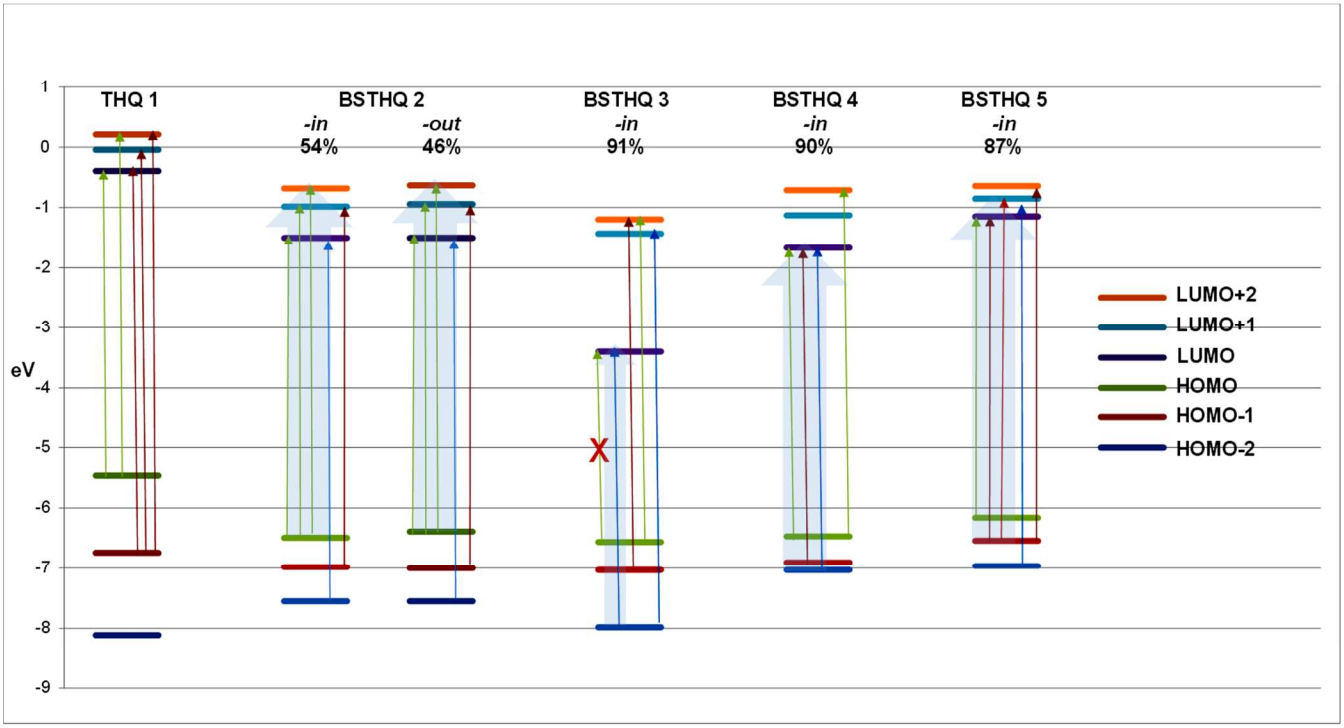

Figure 6. Relative energy (eV) of MOs of compounds **1**-**5** by DFT(B3LYP/6-31+G(d,p)) method in ACN.

Conclusions

A conformational analysis of THQ and its BS derivatives was performed and allowed us to assess that the main contribution to the total UV spectrum comes from the *–in* conformer. The UV spectra of compounds **1**-**5** in acetonitrile, ethanol and dichloromethane were measured. On the basis of experimental and theoretical investigations by the DFT methods, the long-wavelength bands of BSTHQ derivatives have been assigned to π → π* (HOMO → LUMO) transitions were an intramolecular charge transfer from the THQ fragment to the BS group takes place. Nevertheless, for BSTHQ **3**, the

expected HOMO-LUMO transition appears to be optically inactive. In this case, the long-wavelength transition observed was assigned to HOMO-2 → LUMO which suggests an n → π* character.

It was also shown that the calculated electronic transitions as well as the molar absorption coefficients which resulted from applying TD-DFT(B3LYP/6-31+G(d,p)) calculations are in agreement with experimental data. Such correlations were carried out for the first time.

Experimental

Experimental Methods

Compounds **2-5** were synthetized as described elsewhere.[10] All of them were characterized by standard spectroscopic techniques as ^{1}H NMR, ^{13}C NMR, HMBC, HSQC, UV and IR and mass spectrometry. All the physicochemical data were identical to those described before[10] and all of them are presented in the supporting information.

The UV spectra were measured in ethanol, dichloromethane and acetonitrile (all HPLC grade) solutions using 1 cm quartz cells on a UV-71601 Shimadzu spectrophotometer. The concentrations were in the range 1-5x10^{-5} M.

Computational Methods

Conformational and MO calculations have been performed using the Gaussian 09 program.[20] The ground state geometries were fully optimized using the hybrid B3LYP and CAM-B3LYP functional methods, in combination with the 6-31+G(d,p) basis set. The relative population of the conformers was calculated using the Boltzmann population distribution equation.[21] For each optimized structure, a frequency analysis at the same level of theory was used to verify that it corresponds to a minimum in the potential energy surface. For all the minima, the number of imaginary frequencies was zero. The excited state properties were calculated with the time-dependent density functional (TD-DFT) formalism. Contrary to the semi-empirical approaches by which other systems have been studied before,[22] TD-DFT[23-25] is based on first principles and thus has enabled the study of excitation energies, oscillator strengths and polarizabilities of larger systems. TD-DFT in combination with the B3LYP hybrid functional and the 6-31+G(d,p) basis set has previously been shown to provide accurate energies for excited states within 0.2 eV (5 kcal/mol).[21] The polarizable conductor calculation model (C-PCM) of solvation was used in all calculations.[27-28]

Theoretical coefficients (ε_{calc}) have been calculated by the formula (1)[29]:

$$\varepsilon_{cal} = f\, x\, 2.699\, x\, 10^{4} / b, \quad (1)$$

Where b is the line width and f is the oscillator strength.

Acknowledgments

Thanks are due to CONICET, SECYT and FONCYT for financial support. M.V.C., I.M. and A.J.P. acknowledge Doctoral fellowships from CONICET.

Notes and references

[a] INFIQC-Dpto. de Fisicoquímica, Facultad de Ciencias Químicas, UNC, Córdoba, 5000, Argentina.
[b] Departamento de FarmaciaFacultad de Ciencias Químicas – Universidad Nacional de Córdoba.Haya de la Torre esq. Medina Allende. Ciudad Universitaria. Córdoba. Argentina.
* Corresponding author. E-mail: waldemar31@fcq.unc.edu.ar

Electronic Supplementary Information (ESI) available: Characterization of compounds **1-5** and Cartesian Coordinates (Å) obtained from the DFT(B3LYP/6-31+G(d,p)) computational calculations are provided. See DOI: 10.1039/b000000x/

1 M.K. Gupta, Y.S. Prabhakar, *Eur. J. Med. Chem.* **2008**, *43*(12), 2751-2767.
2 J.P. Liou, Z.Y. Wu, C.C. Kuo, C.Y. Chang, P.Y. Lu, C.M. Chen, H.P. Hsieh, J.Y. Chang, *J. Med. Chem.* **2008**, *51*(14), 4351-4355.
3 S.L. Roach, R.I. Higuchi, M.E. Adams, Y. Liu, D.S. Karanewsky, K.B. Marschke, D.E. Mais, J.N. Miner, L. Zhi, *Bioorg. Med. Chem. Lett.* **2008**, *18*(12), 3504-3508.
4 N. Shakya, K.K. Roy, A.K. Saxena, *Bioorg. Med. Chem.* **2009**, *17*(2), 830-847.
5 C.D. Jesudason, L.S. Beavers, J.W. Cramer, J. Dill, D.R. Finley, C.W. Lindsley, F.C. Stevens, R.A. Gadski, S.W. Oldham, R.T. Pickard, C.S. Siedem, D.K. Sindelar, A. Singh, B.M. Watson, P.A. Hipskind, *Bioorg. Med. Chem. Lett.* **2006**, *16*(13), 3415-3418.
6 M.C. Davis, S.G. Franzblau, A.R. Martin, *Bioorg. Med. Chem. Lett.* **1998**, *8*(7), 843-846.
7 L. Garuti, M. Roberti, C. Cermelli, *Bioorg. Med. Chem. Lett.* **1999**, *9*(17), 2525-2530.
8 P.S. Charifson, J.P. Bowen, S.D. Wyrick, A.J. Hoffman, M. Cory, A.T. McPhail, R.B. Mailman, *J. Med. Chem.* **1989**, *32*(9), 2050-2058.
9 S. Lee, S. Oh, G.M. Park, T.S. Kim, J.S. Ryu, H.K. Choi, *Korean J. Parasitol.* **2005**, *43*(3), 123-126.
10 R.J. Pagliero, A.B. Pierini, R. Brun, M.R. Mazzieri, *Lett. Drug. Des. Discov.* **2010**, *7*(6), 461-470.
11 M. Zanger, Diarylsulfone non-nucleosidereverse transcriptase inhibitors of human imunodeficiency virus. US6063790, **2000**.
12 E. Carosati, G. Cruciani, A. Chiarini, R. Budriesi, P. Ioan, R. Spisani, D. Spinelli, B. Cosimelli, F. Fusi, M. Frosini, R. Matucci, F. Gasparrini, A. Ciogli, P.J. Stephens, F.J. Devlin, *J. Med. Chem.* **2006**, *49*(17), 5206-5216.
13 K. Hamamura, T. Oda, T. Kaku, T. Suzaki, Preparation of fused pyrimidine derivative as GnRH antagonists. WO 2006083005 A1 20060810, **2006**.
14 C. Lee, W. Yang, R. G. Parr, *Phys. Rev. B*, **1988**, *37*, 785-789.
15 A. D. Becke, *J.Chem. Phys.* **1993**, *98*, 5648-5652.
16 T. Yanai, D. P. Tew, N. C. Handy, *Chem. Phys. Lett.*, **2004**, *393*, 51-57.
17 X. Liu, D. Yamg, H. Ju., F. Teng, Y. Hou, Z. Lou, *Chemical Physics Lett.*, **2011**, 503, 75-79.
18 C. Hansch, A. Leo, Exploring QSAR. Eds. Fundamentals and Application in Chemistry and Biology, ACS Publications, **1995**.
19 N. M. O' Boyle, A. L. Tenderholt and K. M. Longer, *J. Comp. Chem.*, **2008**, *29*, 839-845.
20 Gaussian 09, Revision B.01, M.J. Frisch, G.W. Trucks, H.B. Schlegel, G.E. Scuseria, M.A. Robb, J.R. Cheeseman, G. Scalmani, V. Barone, B. Mennucci, G.A. Petersson, H. Nakatsuji, M. Caricato, X. Li, H.P. Hratchian, A.F. Izmaylov, J. Bloino, G. Zheng, J.L. Sonnenberg, M. Hada,

M. Ehara, K. Toyota, R. Fukuda, J. Hasegawa, M. Ishida, T. Nakajima, Y. Honda, O. Kitao, H. Nakai, T. Vreven, J.A. Montgomery, Jr., J.E. Peralta, F. Ogliaro, M. Bearpark, J.J. Heyd, E. Brothers, K.N. Kudin, V.N. Staroverov, T. Keith, R. Kobayashi, J. Normand, K. Raghavachari, A. Rendell, J C. Burant, S.S. Iyengar, J. Tomasi, M. Cossi, N. Rega, J.M. Millam, M. Klene, J.E. Knox, J.B. Cross, V. Bakken, C. Adamo, J. Jaramillo, R. Gomperts, R.E. Stratmann, O. Yazyev, A.J. Austin, R. Cammi, C. Pomelli, J.W. Ochterski, R.L. Martin, K. Morokuma, V.G. Zakrzewski, G.A. Voth, P. Salvador, J.J. Dannenberg, S. Dapprich, A.D. Daniels, O. Farkas, J.B. Foresman, J.V. Ortiz, J. Ioslowski, D.J. Fox, Gaussian, Inc., Wallingford CT, **2010**.

21 P. Atkins, J. de Paula, Atkins' Physical Chemistry, Oxford University Press, 7th Edition, **2002**.

22 A.R. Tameev, Z. He, G.H.W. Milburn, A.A. Kozlov, V. Vannikov, A. Puchala, D. Rasala*, Appl. Phys. Lett.* **2002**, *81*(6), 969-971.

23 G. Ricciardi, A. Rosa, S.J.A. Van Gisbergen, E.J. Baerends, *J. Phys. Chem.* **2000**, *104*(3), 635-643.

24 S.J.A. Van Gisbergen, J.A. Groeneveld, A. Rosa, J.G. Snijders, E.J. Baerends, *J. Phys. Chem. A* **1999**, *103*(34), 6835-6844.

25 A. Rosa, E.J. Baerends, S.J.A. Van Gisbergen, E. Van Lenthe, J.A. Groeneveld, J.G. Snijders, *J. Am. Chem. Soc.* **1999**, *121*(44), 10356-10365.

26 J. Llano, L.A. Eriksson, *Pccp. Phys. Chem. Chem. Phys.* **2004**, *6*, 4707-4713.

27 V. Barone, M.Cossi, *J. Phys. Chem. A* **1998**, *102*(11), 1995-2001.

28 M. Cossi, N. Rega, G. Scalmani, V. Barone, *J. Comp. Chem.* **2003**, *24*(6), 669-681.

29 H. Baumann, R.E. Martin, F. Diederich, *J. Compd. Chem*. **1999**, *20*, 396-411.

